CONVERGENCE PROPERTIES OF THE NORMAL MODE OPTIMIZATION AND ITS COMBINATION WITH MOLECULAR GEOMETRY CONSTRAINTS

Petr BOUŘ

Institute of Organic Chemistry and Biochemistry, Academy of Sciences of the Czech Republic, Flemingovo nám. 2, 166 10 Prague 6, Czech Republic; e-mail: bour@uochb.cas.cz

Received December 21, 2004
Accepted June 14, 2005

Optimization in the normal mode coordinates has been established as a useful tool for modeling of vibrational spectra (*J. Chem. Phys.* **2002**, *117*, 4126). In this work the algorithm is extended with the aid of harmonic penalty functions to allow for multiple restraints of geometry parameters, such as bond lengths, bond and dihedral angles, and for simultaneous optimization of more molecules. Additionally, geometry optimization when atomic nuclei are maintained on the constant electrostatic potential surface was implemented and its applications for solvent models are discussed. Model systems include small molecules, water cluster, antiparallel β-sheet peptide containing intermolecular hydrogen bonds, periodic α-helix and a parallel β-sheet segments. The normal mode method provided better numerical stability than the conventional redundant internal coordinates, especially for weakly hydrogen-bonded systems, while the speed of the optimization was found similar as for the Cartesian coordinates.

Keywords: Vibrational spectroscopy; Ab initio calculations; Geometry optimization; Molecular modeling; Vibrational normal modes; Beta sheet, Peptides.

The search for equilibrium molecular structures is one of the principal tasks in the computational chemistry[1]. As a good standard, optimization of the molecular intrinsic (internal) or redundant intrinsic coordinates has been established[2]. For special cases, however, different approaches are necessary. For symmetric cyclic molecules, for example, only mediocre performance of the Z-matrix internal coordinates has been observed if compared to Cartesians[3]. Special attention must be taken if constraints are applied within combined quantum/molecular dynamics methods[4]. Optimization in the Cartesian coordinates is often more numerically stable, even though it takes a longer time on average. Improvements of the step size selection were found necessary for floppy molecules or systems with high average coordination numbers[5]. Other popular choices include normal mode[6], natural[7,8], generalized natural[9], force-constant weighted redundant[10] and

doi:10.1135/cccc20051315

delocalized[11] coordinates, or combinations of different types[12,13]. Direct methods for the location of the lowest energy point on a potential surface crossing were proposed[14,15]. Typically, methods based on internal coordinates related to the Cartesian space by a non-linear transformation are more efficient than the canonic normal modes[16]. However, this may be different for complex systems, like those containing weak hydrogen bonds, where the normal mode coordinate optimization was shown to converge more smoothly than the methods based on the internal coordinates[17].

But rather than a search for general optimization method, this study concentrates on particular convergence properties of the normal mode algorithm and simultaneous control of the normal mode and geometry parameters. The reason for this is that the choice of the harmonic normal mode vibrational coordinates is essential and inevitable for simulations of infrared spectra because they provide a direct control over the relaxation of vibrational motions responsible for absorption intensities[17]. Additionally, by fixing some normal modes, a reasonable degree of control could be achieved also over geometrical parameters[17]. This enabled simulations of vibrational circular dichroism spectra of nucleic acids[18] and simplified modeling solvent of solvent spectral response[19,20]. Similarly, the normal mode techniques have to be utilized for localization of transition states and following reaction paths[21]. However, direct simultaneous control over geometry and vibrational coordinates has not been investigated yet.

Performance of the normal modes is generally comparable to Cartesian coordinates as the two coordinate sets span the same linear vector space. In simplest implementation they provide exactly same optimization trajectories, while they deviate for case when non-linear transformation operations are used in the optimization cycle[6]. These involve, for example, the maximum step criterion or application of rational function optimization (RFO)[22,23] method involving trust radius estimation[1]. As shown below, these factors can play a significant role for optimizations of strongly anharmonic systems, where the initial geometry deviates significantly from the minimum, such as hydrogen-bond complexes.

The pure normal mode coordinate scheme, as introduced originally[1,17], does not enable one to fix specific internal coordinates, such as bond lengths or angles. This handicap is removed in the present implementation, where the method is also extended to allow for multiple coordinate restrictions. This may be useful, for example, for regular peptide structures, where it is desirable to keep the torsion angles restricted to those found by X-ray crystallography. Although the ultimate goal of molecular modeling still remains to obtain consistently the true energy minimum of the studied sys-

tems, many molecular properties are often simulated for smaller fragments only. The fragments cannot be stabilized by longer-range "natural" interactions, while an arbitrary stabilization via the constraints is often sufficient for the modeling. For vibrational problems, it is obviously desirable to maintain the mastering of the normal mode motion in addition to the internal-coordinate control, allowing one to approach the one-dimensional energy minima of important (typically higher-energy) modes visible in the Raman or absorption spectra. A penalty-function approach[24] is used for the coordinate constraints, because of their simplicity and in order to achieve a flexible degree of coupling between the normal and internal coordinates, instead of the more common method of Langrange multipliers[25] used for the internal[26] and Cartesian[27] sets.

Another interesting problem is a search for the optimal geometry under external electrostatic field. The dominance of the electrostatic forces in the solute-solvent interactions has been recognized a long time ago[28] and utilized in many simplified solvent models[29–31]. Typically, the solvent environment is modeled by a cavity created around the solute, while the field comes from arbitrary charges distributed on the cavity surface. The size of the charges is determined self-consistently, taking into account specific boundary conditions for the external field and the molecular response. Proper involvement of the solvent effects in quantum computations was found essential for many molecular properties, such as solvation Gibbs energies[32], optical rotations[33] or vibrational frequencies[34]. Recently, vibrational frequency shift for small polar molecules was related to the electrostatic potential at the nuclei[35] and the influence was qualified on the basis of the vibrational transition charges concept[36]. In an empirical model, the electrostatic approximation dramatically decreased the computational time needed for correct simulation of the infrared absorption of the analytically important amide I peptide mode[19]. For *N*-methylacetamide, the amide mode frequencies were found to be determined by the atomic electrostatic potentials for polar solvents[37,38]. Thus in context with the normal mode optimization algorithm it appears natural to include also the possibility to control the electrostatic potential at the nuclei, and, consequently, the solvent shifts of vibrational frequencies in solvent–solute systems.

The manuscript is organized as follows. In the next methodological section, the normal mode optimization algorithm is briefly reviewed and the implementation of the constraints described above is elaborated. In the results section, typical convergence behavior of the normal mode method is compared with optimizations based on Cartesian coordinates for furan, adamantane derivative, cyclohexane and a water cluster. Then, the behav-

ior of the method is tested on examples comprising optimization of an antiparallel β-sheet segment with fixed dihedral angles, models of periodic protein α-helical and parallel β-sheet structures with multiple constraints, and simultaneous optimization of two molecules. Finally, an example of optimization within an external field under constant electrostatic potential at the nuclei is given. Some mathematical and computational details are kept as the supplementary material (http://cccc.uochb.cas.cz/Vol/70/No09/20051315.html).

METHOD

The Normal Mode Coordinates

The normal mode coordinates (q_i, $i = 1, 3N - 6$ ($3N - 5$ for linear molecules), where N is the number of atoms) are related to the Cartesian atomic displacements $\{X_{\lambda\alpha}, \lambda = 1...N, \alpha = x, y, z\}$ by

$$\mathbf{X} = \mathbf{S}\cdot\mathbf{q} \qquad (1)$$

where the **S**-matrix is obtained via diagonalization of the harmonic vibrational Hamiltonian[39,41]. Within the harmonic approximation the normal modes are independent and provide distinct spectral responses. Using the linear transformation of coordinates given above, the search of the energy minimum can be realized in the normal space. For example, for each optimization point i, the normal mode gradient $\mathbf{g}^{(i)}$ can be obtained from the Cartesian gradient $\mathbf{G}^{(i)}$:

$$\mathbf{g}^{(i)} = \mathbf{S}^t\cdot\mathbf{G}^{(i)}. \qquad (2)$$

Details of the implementation have been given elsewhere[17]. As shown therein, this procedure is not always the fastest optimization method, nevertheless exhibits an excellent numerical stability and gives the opportunity to directly constrain or relax the modes acting in the spectra.

Although the QGRAD program provides many possibilities how the Hessian matrix (**f**) can be handled, for the examples presented in this study a PM3 initial guess was used and continuously updated with the BFGS[40] formula for (i + 1) step

$$\mathbf{f}^{(i+1)} = \mathbf{f}^{(i)} - \left(\frac{\Delta\mathbf{g}^{(i)^t}\Delta\mathbf{g}^{(i)}}{\mathrm{d}\mathbf{x}^{(i)}\cdot\Delta\mathbf{g}^{(i)}} + \frac{(\mathbf{f}^{(i)}\cdot\mathrm{d}\mathbf{x}^{(i)})^t\,\mathrm{d}\mathbf{x}^{(i)}\cdot\mathbf{f}^{(i)}}{\mathrm{d}\mathbf{x}^{(i)}\cdot\mathbf{f}^{(i)}\cdot\mathrm{d}\mathbf{x}^{(i)}} \right)$$

where with Cartesian displacements $d\mathbf{x}^{(i)} = \mathbf{x}^{(i)} - \mathbf{x}^{(i-1)}$ and the gradient differences $\Delta\mathbf{g}^{(i)} = \mathbf{g}_c{}^{(i)} - \mathbf{g}_c{}^{(i-1)}$. Trial calculation of the initial Hessian at the same level as the gradient led usually to faster convergence, but this could not be done for large systems and the acceleration was minor for the anharmonic systems studied here. Ideally, the Hessian can be fully recalculated at each step ab initio, which, however, brings even bigger computational burden.

Constraints of Geometric Parameters

Bond lengths, angles and torsional angles are intrinsic coordinates that can be encountered most frequently in chemistry. Their control within the normal mode algorithm can be achieved by adding penalty functions as harmonic terms to the molecular energy (E), and by minimizing the sum:

$$S = E + \sum_{j=1}^{N_P} b_j (p_j - p_j^0)^2 \rightarrow \min \qquad (3)$$

where the index j runs over N_P parameters (distances, angles, torsions), p_j and p_j^0 are the actual and desired values of parameter j, respectively; b_j is an arbitrary barrier. If the energy is calculated in atomic units, distances measured in Å, and angles in degrees, a reasonable value of the barrier is around unity ($b_j \approx 1$) for bond lengths and $b_j \approx 10^{-2}$ for the angles. As shown below, however, the optimization path is relatively insensitive to parameter variations. Expression (*3*) is obviously same as the harmonic energy terms used in molecular dynamics. In order to use it for geometry constraints within the normal mode technique, Cartesian gradient $\mathbf{G}'$ and second-energy derivatives (Hessian) $\mathbf{F}'$ are modified:

$$G'_{\lambda\alpha} = \frac{\partial S}{\partial R_{\lambda\alpha}} = G_{\lambda\alpha} + 2\sum_{j=1}^{N_P} b_j (p_j - p_j^0) \frac{\partial p_j}{\partial R_{\lambda\alpha}} \qquad (4)$$

$$F'_{\lambda\alpha,\mu\beta} = \frac{\partial^2 S}{\partial R_{\lambda\alpha} \partial R_{\mu\beta}} = F_{\lambda\alpha,\mu\beta} + 2\sum_{j=1}^{N_P} b_j (p_j - p_j^0) \frac{\partial^2 p_j}{\partial R_{\lambda\alpha} \partial R_{\mu\beta}} + 2\sum_{j=1}^{N_P} b_j \frac{\partial p_j}{\partial R_{\lambda\alpha}} \frac{\partial p_j}{\partial R_{\mu\beta}} \qquad (5)$$

where $R_{\lambda\alpha}$ denotes an α-coordinate (α = 1, 2, 3) of atom λ. For the normal modes, new coordinates and frequencies can be obtained self-consistently by diagonalizing the Hessian (*5*) and the rest of the algorithm remains the same as for the unrestricted optimization[17]. In all presented examples the

energy contains the penalty function – note that this part disappears for complete convergence.

Coordinate Derivatives

For a sequence of 4 atoms, distances, angles and torsional angles may be defined with the aid of vectors $\mathbf{v}_i$ pointing along the bonds as[41]

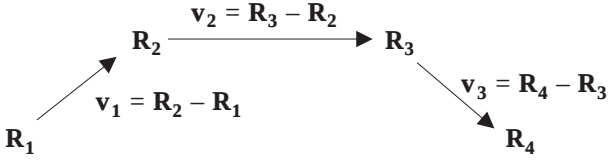

$$p = (\mathbf{v}_1^{\,2})^{1/2} = v_1 \text{ (distance)} \tag{6}$$

$$p = \arccos(o);\; o = -\frac{\mathbf{v}_1 \cdot \mathbf{v}_2}{v_1 v_2} \text{ (bond angle)} \tag{7}$$

$$p = \operatorname{sign}\arccos\left(\frac{\mathbf{a} \cdot \mathbf{b}}{ab}\right) = \operatorname{sign}\arccos(o) \text{ (torsion angle)} \tag{8}$$

with vector products $\mathbf{a} = \mathbf{v}_1 \times \mathbf{v}_2$ and $\mathbf{b} = \mathbf{v}_2 \times \mathbf{v}_3$. The usual sign convention is adopted (sign = –1 for $\mathbf{a}\cdot\mathbf{v}_3 < 0$, else sign = 1), which provides positive angles for the right-handed arrangement of the bonds[42]. The only non-zero first derivatives of the bond vectors are

$$\frac{\partial \mathbf{v}_1}{\partial \mathbf{R}_2} = \frac{\partial \mathbf{v}_2}{\partial \mathbf{R}_3} = \frac{\partial \mathbf{v}_3}{\partial \mathbf{R}_4} = -\frac{\partial \mathbf{v}_1}{\partial \mathbf{R}_1} = -\frac{\partial \mathbf{v}_2}{\partial \mathbf{R}_2} = -\frac{\partial \mathbf{v}_3}{\partial \mathbf{R}_3} = \mathbf{E} \tag{9}$$

with the 3 × 3 unit matrix **E**, while the second derivatives vanish completely. Thus it appears convenient to break down the expressions 4–5 up to the derivatives of the vectors $\mathbf{v}_1 - \mathbf{v}_4$, which is derived in detail in the supplementary material (Eqs 1S–28S).

Constraints Involving Two or More Parameters

Similarly, by adding an additional quadratic energy term, any two geometrical parameters, *i* and *j*, can be coupled. In most cases, this is meaningful for chemically analogous coordinates of the same type, such as those in final-sized models mimicking periodic structures. The energy term becomes

$$\Delta E = b_{ij}(p_i - p_j)^2 \tag{10}$$

and corresponds to changes in gradient

$$G_{\lambda\alpha} = 2b_{ij}(p_i - p_j)\left(\frac{\partial p_i}{\partial R_{\lambda\alpha}} - \frac{\partial p_j}{\partial R_{\lambda\alpha}}\right) \tag{11}$$

and second derivatives

$$F_{\lambda\alpha,\mu\beta} = 2b_{ij}(p_i - p_j)\left(\frac{\partial^2 p_i}{\partial R_{\lambda\alpha}\partial R_{\mu\beta}} - \frac{\partial^2 p_j}{\partial R_{\lambda\alpha}\partial R_{\mu\beta}}\right) + \\ + 2b_{ij}\left(\frac{\partial p_i}{\partial R_{\lambda\alpha}} - \frac{\partial p_j}{\partial R_{\lambda\alpha}}\right)\left(\frac{\partial p_i}{\partial R_{\mu\beta}} - \frac{\partial p_j}{\partial R_{\mu\beta}}\right). \tag{12}$$

Geometry Optimization with Constant Potential at the Nuclei

For reasons indicated in the introduction, we may wish to keep the electrostatic potential φ_j at each nucleus *j* (*j* = 1...N_{AT}, N_{AT} is number of atoms) constant. For example, the potential can mimic the influence of the solvent. Similarly as for the geometric parameters, a quadratic energy term is added to the total molecular energy

$$\Delta E = \kappa \sum_{j=1}^{N_{AT}} (\varphi_j - \varphi_j^0)^2 \tag{13}$$

where κ is an arbitrary constant, and φ_j and φ_j^0 is the actual and desired potential, respectively.

Accordingly, the gradient and second derivatives will be modified, so that

$$\Delta G_{\lambda\alpha} = 2\kappa \sum_{j=1}^{N_{AT}} (\varphi_j - \varphi_j^0) \frac{\partial \varphi_j}{\partial R_{\lambda\alpha}} \tag{14}$$

$$\Delta F_{\lambda\alpha,\mu\beta} = 2\kappa \sum_{j=1}^{N_{AT}} (\varphi_j - \varphi_j^0) \frac{\partial^2 \varphi_j}{\partial R_{\lambda\alpha} \partial R_{\mu\beta}} + 2\kappa \sum_{j=1}^{N_{AT}} \frac{\partial \varphi_j}{\partial R_{\lambda\alpha}} \frac{\partial \varphi_j}{\partial R_{\mu\beta}} . \tag{15}$$

For the case when the field is realized by an ensemble of N_C point charges $\{q_i, i = 1...N_C\}$, e.g. by effective charges of solvent atoms, the potential is

$$\varphi_j = \sum_{i=1}^{N_C} \frac{q_i}{r_{ji}} \tag{16}$$

where $r_{ji} = |\mathbf{R}_j - \mathbf{r}_i|$, $\mathbf{R}_j$ and $\mathbf{r}_i$ are the nuclei and charge positions, respectively. Thus the potential derivatives become

$$\frac{\partial \varphi_j}{\partial R_{\lambda\alpha}} = -\sum_{i=1}^{N_C} \frac{q_i}{r_{ji}^3} (R_{j\alpha} - r_{i\alpha}) \delta_{j\lambda} \tag{17}$$

$$\frac{\partial^2 \varphi_j}{\partial R_{\lambda\alpha} \partial R_{\mu\beta}} = -\sum_{i=1}^{N_C} \frac{q_i}{r_{ji}^3} \delta_{j\lambda} \delta_{j\mu} \delta_{\alpha\beta} + 3 \sum_{i=1}^{N_C} \frac{q_i}{r_{ji}^5} (R_{j\alpha} - r_{i\alpha}) (R_{j\beta} - r_{i\beta}) \delta_{j\lambda} \delta_{j\mu} . \tag{18}$$

If the dependence is solved self-consistently, we might want to consider also the dependence of the charges on nuclei positions. However, this is not trivial and for the purpose of this study we neglected the dependence setting

$$\frac{\partial q_i}{\partial R_{\lambda\alpha}} = \frac{\partial^2 q_i}{\partial R_{\lambda\alpha} \partial R_{\mu\beta}} = 0 .$$

It should be emphasized that for N atoms the full number of $3N$ normal modes must be included in the constant potential optimization, including the molecular rotations and translations, in order to obtain numerically stable and meaningful results. Additionally, since these collective modes are generally associated with non-zero vibrational frequencies in the external electrostatic potential, no arbitrary projection of the force field[43] before the diagonalization can be applied.

The equations given above have been implemented in the home-made program QGRAD, while the ab initio calculations were made with the GAUSSIAN [44] program. Also with GAUSSIAN, the optimizations with redun-

dant internal coordinates were performed for comparison with the normal mode procedures.

RESULTS AND DISCUSSION

Cartesian versus Normal Mode Coordinates

As pointed above, the normal mode and Cartesian coordinates form both a complete basis in the same linear vector space. The equivalence, however, transfers into the same optimization trajectory only under specific conditions, namely when the optimization algorithm based on the harmonic expansion does not contain non-linear transformations. This can be achieved for simple systems, as shown for furan and bromochlorofluoroadamantane molecules in Fig. 1. For both systems the PM3 Hessian was used as an initial guess of the force field. For furan and Br–Cl–F–adamantane, PM3 and HF/3-21G optimized geometries were used as starting points, and the optimizations were performed at the HF/4-31G and PM3 levels, respectively. The minimization was made with the QGRAD program; ab initio energies and gradients were obtained from Gaussian. As can be seen in Fig. 1, the optimization trajectory for the Cartesian coordinates (i), as indicated by the energy, coincides with the normal mode trajectory (ii). The deviation between these two methods at the last points of the optimizations is given by the final numerical precision of current implementation, if for example, the energy is recorded to 9 decimal places (Note that 4 decimal places are usually satisfactory for chemical accuracy). Similarly, when the updating of the Cartesian force field along the optimization path is switched on, the performances of the Cartesian (iii) and normal mode (iv) based optimizations are equal within the numerical accuracy, both for the furan and adamantane derivative. As expected, the updating of the second energy derivatives also accelerates the convergence, decreasing the number of optimization steps approximately by a factor of two. In fact, the implementation of the fixed, non-updated Hessian is extremely inefficient and can be seldom recommended in practice.

The rational function correction[22,23] is a typical example of a non-linear perturbation in the optimization algorithm which causes deviations between the Cartesian and normal mode paths. Indeed, if the RFO method is applied, the two coordinate sets are not equal as can be seen in Fig. 2 for the two test molecules. The optimizations were done under same conditions as for Fig. 1, with the Hessian update, except for the Cartesian-RFO scheme (e in Fig. 2), for which the GAUSSIAN program was used. For the

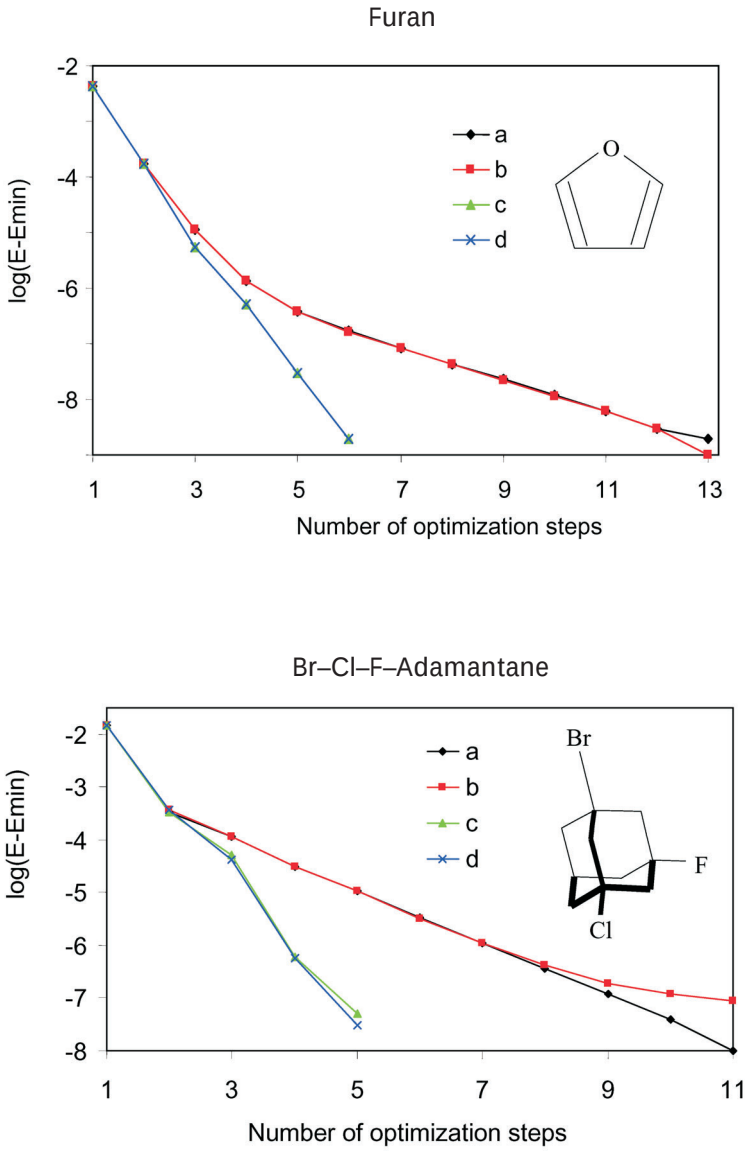

FIG. 1

The dependence of the relative energy on the number of optimization steps for furan (top) and Br–Cl–F-adamantane (bottom) for pure (a) Cartesian mode and (b) normal optimization methods, and when the update of the Hessian was switched on (c, d, for the Cartesian and normal coordinates, respectively)

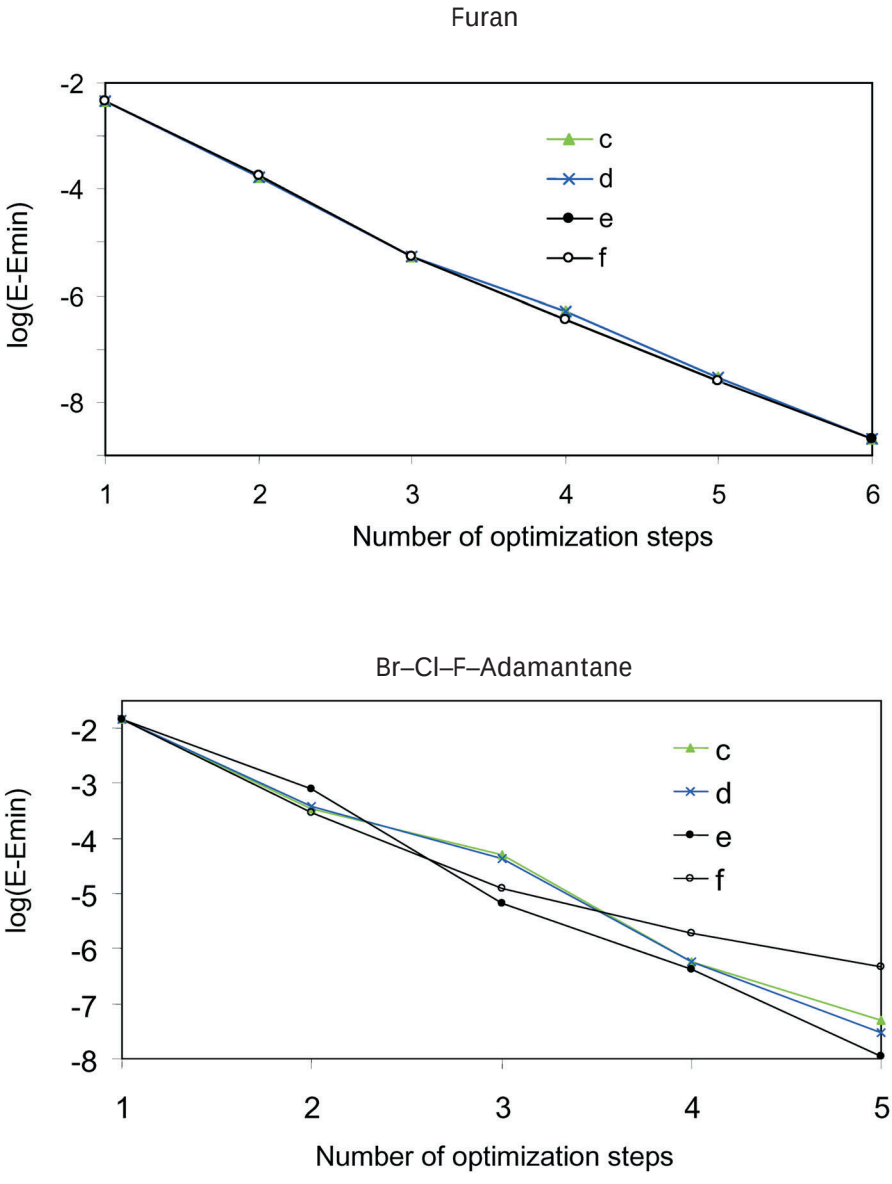

FIG. 2
The dependence of the energy on the number of optimization steps for furan (top) and Br–Cl–F–adamantane (bottom) for the Cartesian (c, e) and normal mode (d, f) optimizations with continuous updating of the Hessian, with (e, f) and without (c, d) the RFO correction

RFO trajectories, we can observe a difference between the furan and Br–Cl–F–adamantane molecules. For the former, both the normal and Cartesian coordinates provide approximately same trajectories, while for the latter the RFO trajectories (e, f in Fig. 2) noticeably differ, the Cartesian method providing somewhat faster convergence. This can be attributed to greater rigidity of the furan system, since the lowest-frequency harmonic vibrational mode was calculated at 507 cm^{-1} while the lowest wavenumber for Br–Cl–F–adamantane is 63 cm^{-1}.

The RFO method or its analogue, combined with the limit of the maximum step size, must be used for a vast majority of molecular optimizations, which often involves incomplete or non-positively definite Hessian. This is, for example, the case of the cyclohexane optimization recorded in the upper part of Fig. 3. For the starting geometry (with arbitrarily chosen torsion angles within the six-membered ring of –1, –1, –14, 44, –42 and 19°), two negative Hessian eigenvalues (corresponding to imaginary frequencies i353 and i242 cm^{-1}) were calculated at the PM3 level, which obviously prevents direct use of the quadratic approximation both for the normal and Cartesian coordinates. Even with the RFO potential approximation, the optimizations become rather tedious, requiring about 40–50 steps to converge (a, b in Fig. 3). At later stages of the optimization, the normal mode method (b) seems to converge faster, in contrast to Br–Cl–F–adamantane (cf. Fig 2, bottom). For cyclohexane, both the normal mode and Cartesian optimizations are significantly slower than the internal redundant coordinates included in Fig. 3 as trace c. This corresponds to earlier observations, where the internal coordinates provide usually superior results for covalent systems[7,17].

Yet the convergence properties of the different optimization schemes change again for weakly-bonded systems, as shown for a cluster of three water molecules in the lower part of Fig. 3. For the initial geometry, the water molecules were arbitrarily chosen so that mass centers were about 3.4 Å apart and approximately in a triangle. At the PM3 level, the lowest negative Hessian eigenvalue corresponded to i29 cm^{-1}, lower in absolute value than for cyclohexane. Nevertheless, not only took optimization of the water several times more steps, but also qualitative behavior of the three optimization techniques changed. The Cartesian method as implemented in GAUSSIAN (a) provided again slowest convergence, with apparent instabilities at the end of the optimization. But the normal mode method (b in Fig. 3) converged much faster after about 100 steps and even earlier than the redundant scheme (trace c). In this particular case, the redundant method provided a local energy minimum different from those obtained by the Cartesian and normal mode methods. The redundant coordinates had

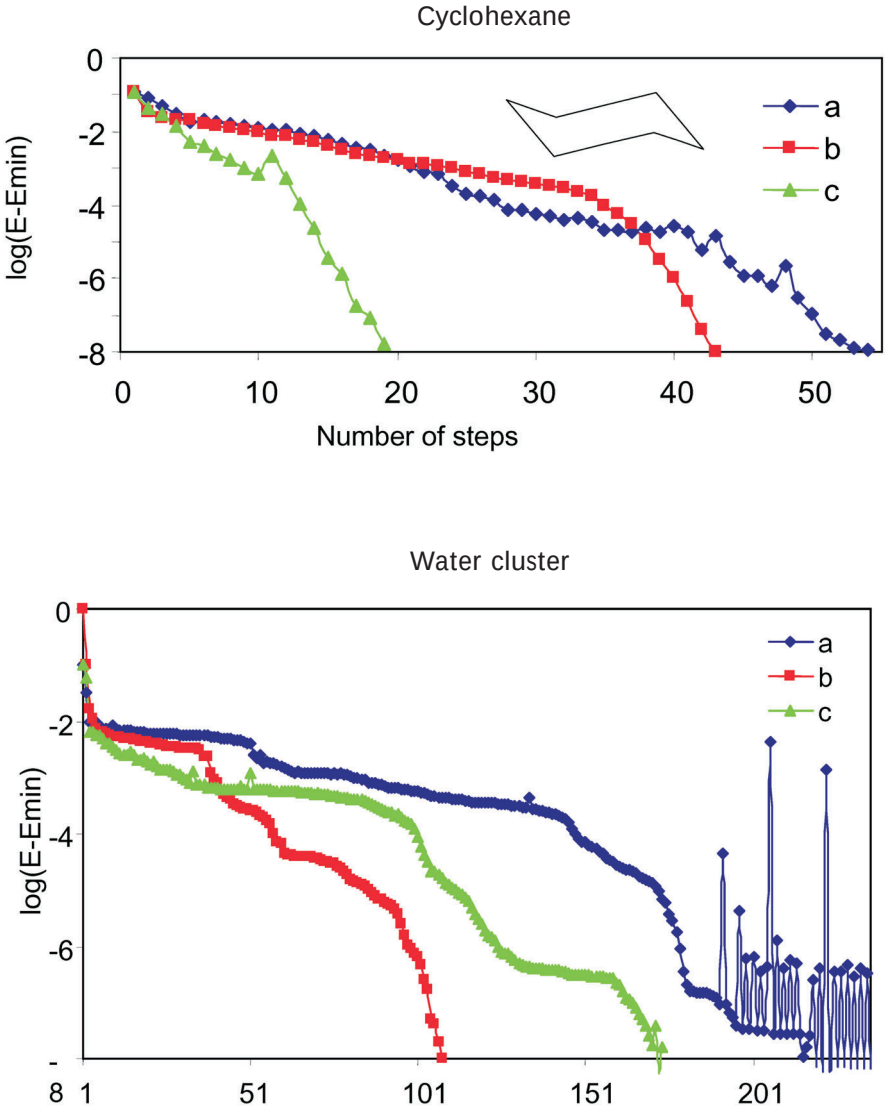

FIG. 3

The energy convergence for cyclohexane (top) and a water cluster (bottom), obtained with the Cartesian (a), normal mode (b) and internal (c) coordinates. Hessian updating and RFO potential smoothing were applied

to be also redefined three times during the optimization run and the computation manually restarted. Thus, in accordance with previous observation, the normal mode method seems to be especially suitable for weak, e.g. hydrogen-bond complexes; in addition, its stability provides the ability to control the vibrational modes.

Antiparallel β*-Sheet Segment*

A six-amide segment (see Fig. 4 for geometry) based on L-alanine polymer was chosen as a typical example of systems that can be encountered in molecular biology modeling. By controlling the torsional angles of the carbonyl group (τ, τ′ in the figure), one can model the overall twist of the β-sheet, and its secondary and tertiary structure[45,46]. Although the system is quite stable in vacuum[47], unlike those of other protein forms[49], the computational task of obtaining the equilibrium geometry is quite difficult. For illustration of the coordinate dependence, the RHF/6-31G level of approximation was chosen. The HF method provides smooth analytical gradients, unlike the DFT methods using integrations grids, for example, which might bias the coordinate dependence.

The starting geometry was derived from a planar sheet with $\tau \approx \tau' \approx 0°$, while the constraints of $\tau = \tau' = 20°$ were imposed during the energy minimization, with $b = 0.01$ (Eq. (*3*)). Such a restricted optimization can be done both with the normal mode as well as with the internal coordinate-based algorithms. As can be seen from the dependence of the total en-

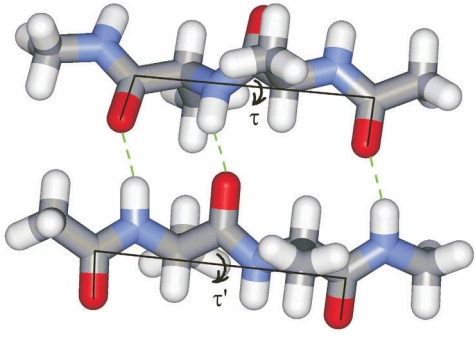

FIG. 4
The antiparallel β-sheet peptide used in the constrained optimization. The starting values of the arbitrary torsional angles $\tau \cong \tau' \cong 0°$ were restrained to $\tau = \tau' = 20°$. The hydrogen bonds between the two Ac-(L-)-Ala-(L-)-Ala-NH-Me peptide chains are indicated by the green dashed line

ergy on the number of the optimization steps in Fig. 5, the redundant internal method exhibits numerical instabilities. Moreover, it never converges completely, oscillating (ca. ±0.01 hartree) after about 200 steps around an average value of the energy. A non-redundant set of intrinsic coordinates (note that many choices of the Z-matrix are possible) converges reasonably well at initial stages of the optimization. However, the convergence stops around the 80th step and starts to oscillate (ca. ±0.0002 hartree). On the other hand, the normal mode optimization provides a smooth convergence. Even for the latter method, however, the number of optimization steps is rather enormous compared with usual covalent-bond systems. About 75 steps are needed to achieve an energy error smaller than 10^{-3}, 188 steps for $\Delta E < 10^{-5}$ and 227 steps for $\Delta E < 10^{-6}$. Complete convergence ($\Delta E < 10^{-8}$) was obtained after about 288 steps. The convergence thus accelerates (at least in the logarithmic scale) at final stages of the optimization when the potential energy surface becomes more quadratic, while the difficulties in initial stages reflect the shallow anharmonic potential of the inter-

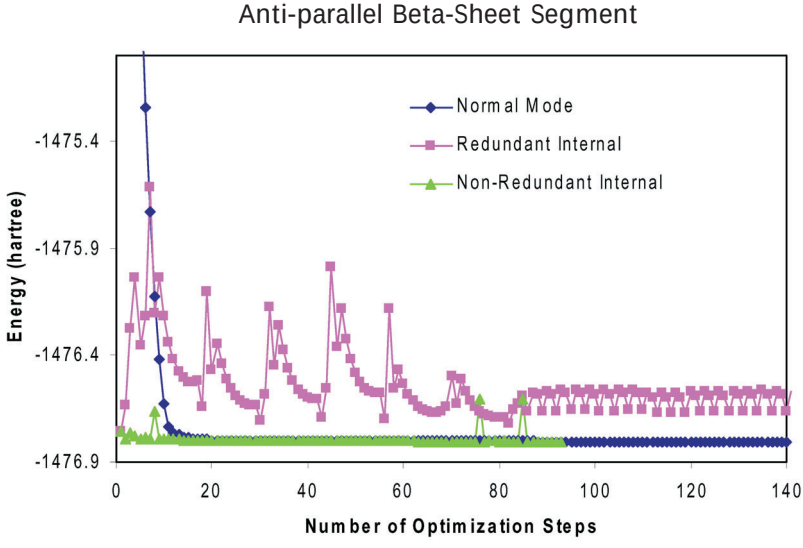

FIG. 5

The convergence of the total energy during the constrained optimization of the antiparallel β-sheet segment displayed in Fig. 4: comparison of the normal mode, internal and redundant (Gaussian 03/version B02)[44] methods. Note that the starting total energy in normal modes is higher since it contains the arbitrary harmonic terms of Eq. (*3*)

molecular interactions. Similar problems were observed also for hydrogen-bonded water complexes[17]. Nevertheless, we can conclude that the normal mode method does provide a numerically stable means for the treatment of these systems.

One may wish to know the influence of the penalty barrier (cf. Eq. (*3*)) on the quality of the convergence. For most cases it seems to be quite minor and can vary within an interval of several orders, as can be documented in Fig. 6 where the initial stages of the antiparallel β-sheet optimization are shown for three values of *b* (0.01, 0.001 and 0.0001). For the two highest values, the constrained angles quickly achieve the desired limit, which is controlled by the maximal allowed displacement rather than by the parameter itself. For the smallest value, the constraints are approached more

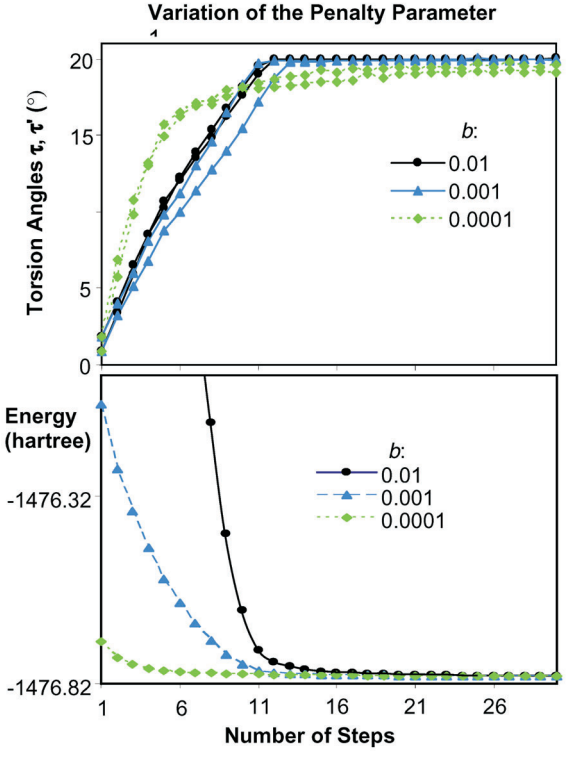

FIG. 6
Initial optimization phases of the antiparallel β-sheet for three values of the penalty parameter (*b*, Eq. (*3*)): the dependence of the constrained torsion angles (defined in Fig. 4) and the total energy on the number of optimization steps

slowly; nevertheless, because of the immense number of steps required for complete optimization, it has a small influence on the total number of steps and final outcome. When the starting geometry parameters deviate significantly from the desired values, or for complicated multiparameter fit (see below), it seems reasonable to use rather small magnitudes of the barriers in order to avoid covalent bond splitting and atom overlapping.

It should be noted, both for the normal mode and for the redundant coordinate methods, that the speed of the convergence depends on other details of the implementation, which are quite numerous and may be optimized for each system separately. Here, comparable "default" parameters were chosen, including a low-level estimation of the Hessian and its continuous update during the minimization using Cartesian gradients and a maximum step of about 0.1 Å.

Parallel β*-Sheet and* α*-Helical Peptides*

Parallel β-sheets can be found in nature quite often, although less frequently than the antiparallel sheets, while α-helix is perhaps the most notoriously known protein secondary structure[48]. The octaamides (see Fig. 7 for the starting geometry) mimicking these structures were thus chosen as important examples of periodic systems. The periodicity conditions cannot be imposed conventionally in the redundant coordinates. Using the normal mode algorithm, all {φ,ψ} dihedral angles may be required to be the same even if their values are not specified. Obviously, under this constraint, all

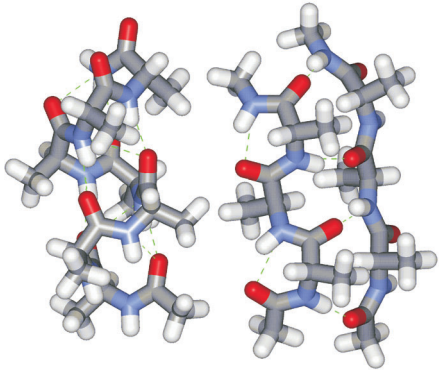

FIG. 7
The α-helical (left) and parallel β-sheet (right) L-alanine-based octaamide peptides. Inter- and intramolecular hydrogen bonds are indicated by the dashed green lines

other coordinates will not follow the infinite periodicity; nevertheless, the {φ,ψ} angles are the most relevant for the modeling of physical or physiological protein properties. Starting values of the angles were set uniformly to –57 and –47° for all the 7 amino acid residues in the α-helix. Initial geometry of the β-sheet was slightly distorted from the planar (periodic) conformation and the angles were more dispersed, with $\varphi \in (-160,-82)$ and $\psi \in (75,165)$. Since the α-helical structure is not stable in vacuum[49], the COSMO [30] continuum solvent model was applied to both forms, using the same HF/6-31G level of approximation as for the previous example. The value of $b = 10^{-5}$ was used in Eq. (*10*).

For the parallel β-sheet model, we can follow the initial convergence in Fig. 8. Clearly, the energy smoothly decreases during the optimization run, while small oscillations are apparent for some angle values. Nevertheless, the angles convincingly converge to common values, i.e. to φ = –113° and ψ = 116°. These reasonably well agree with the standard values of –119 and 113° tabulated for the planar parallel β-sheet[48].

Similar and somewhat faster (within fewer number of optimization steps) convergence of the total energy and the torsion angles can be observed also for the α-helix in Fig. 9. Here, the main chain angles optimized to φ = –65° and ψ = –38°, i.e. they rather significantly deviate from the canonical values of (–47,–57°) for this structure. Although the α-helical hydrogen-bonding pattern did not change, the optimized values approached rather those tabulated for standard 3_{10}-helix (–60,–30)[48]. This may be accounted for by inadequacies of the model, mainly by the insufficient length of the peptide (it is known that shorter peptide sequences do not form stable α-helices) as well as by the continuous approximation of the solvent, unable to simulate the strong hydrogen-bond solvent–solute stabilization interactions[49]. In this case the speed of the convergence was more influenced by the magnitude of the penalty barriers; particularly for high values the convergence speed sharply decreases (details are given in the supporting section). At the initial stages of the optimization the angle values oscillates which suggest that the algorithm does not follow the lowest-energy path too faithfully. However, at the harmonic limit this seems inevitable, and control computations with independent molecular dynamics software provided similar dependence of analogous optimization tasks.

Simultaneous Optimization of More Molecules

Optimization of two or more molecules with coupled parameters ranks among more complex computational tasks. Nevertheless, molecular proper-

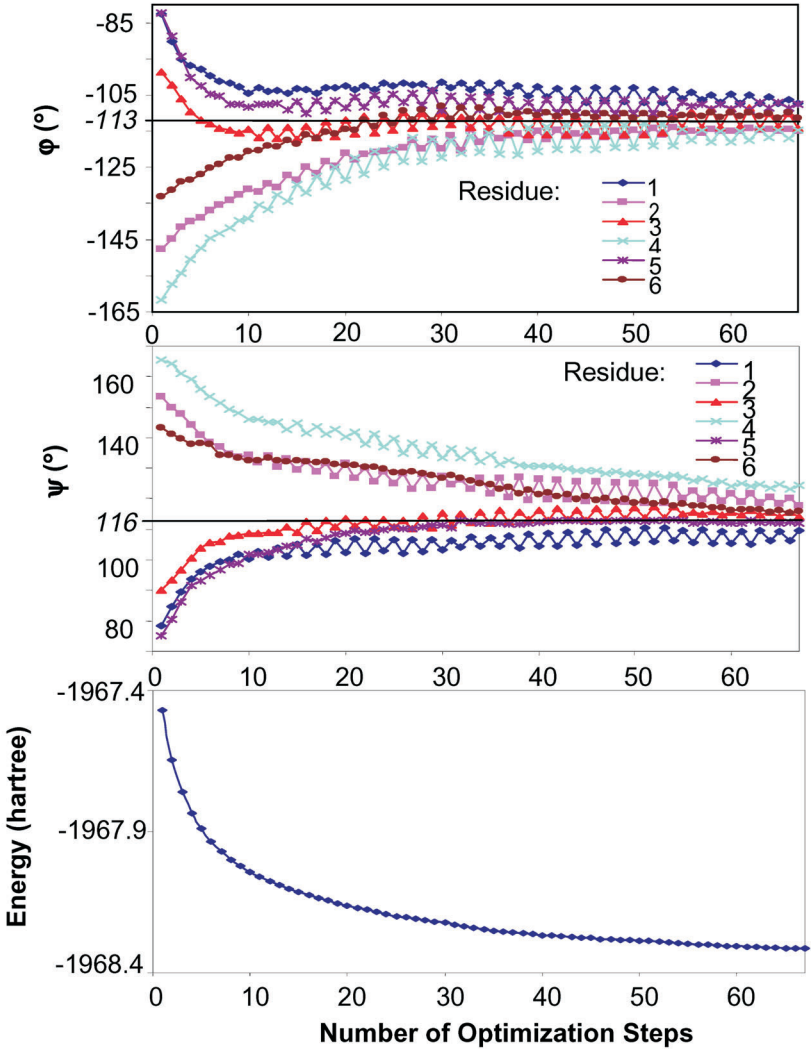

FIG. 8

The dependence of the main chain peptide torsion angles (φ,ψ) and the total energy on the number of optimization steps for the parallel β-sheet peptide (Fig. 7 right). The angles φ and ψ were constrained so that each converged to the same value, but this value was not specified and no other constraints were imposed. The HF/6-31G/COSMO level of approximation was used. Only initial phase of the optimization is shown. The values converged to (φ = –113°, ψ = 116°), although numerical instabilities were observed at later stages due to the inaccurate gradients provided by the solvent COSMO model

ties of bigger systems are often predicted based on computations of smaller fragments[49–52]. The selected example thus simulates situation, where low-frequency normal mode motions are fixed (so that the structure base on a natural system does not collapse) and, at the same time connecting molecular parts fit together, i.e. coordinates of overlapping atoms are dependent. Particularly, a tetraamide model system displayed in Fig. 10 on the left was chosen, mimicking a twisted antiparallel (-sheet systems often found in natural proteins[53,54]. The initial peptide main-chain torsion angles (φ,ψ)

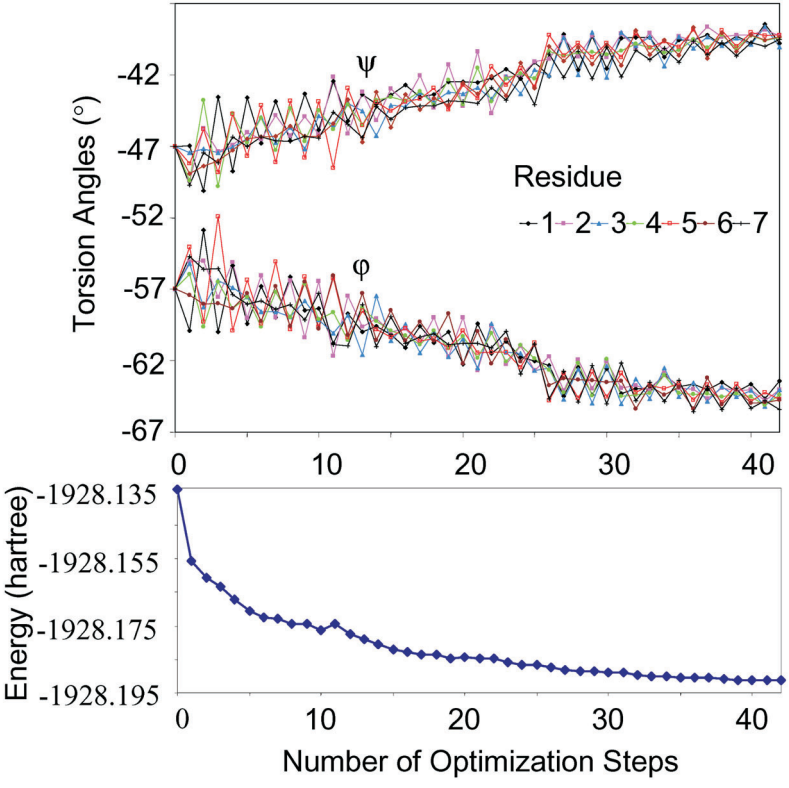

FIG. 9

The dependence of the main chain peptide torsion angles (φ,ψ) and the total energy on the number of optimization steps for the α-helical peptide (Fig. 7 left). The angles φ and ψ were constrained to maintain the same value; no other constraints were required. The HF/6-31G/COSMO level of approximation was used. Only initial phase of the optimization (converged finally for φ = –65° and ψ = –38°) is shown

were chosen as (–110,120) and (–64,153) for the two strands, respectively. Then the fragments were subjected to restricted optimization, with the methodology described above. The QGRAD program[17] was used for normal mode-based optimization, while the energies and gradients were obtained with GAUSSIAN [44], at the PM3 level of approximation. In the optimization routine, the two fragments were treated as a super-molecule, parameters (energy, gradient, Hessian) were obtained from the two fragments; thus, technically, the procedures described above could be used.

On the left hand side of Fig. 11, the energy and geometric parameter changes during the optimization run can be seen, with constraints involving normal modes (modes with wavenumbers within –300 and 300 cm^{-1} were fixed) and the distance (1–2), bond angles (1–2–3, 2–3–4) and torsion angles (1–2–3–4) defined in Fig. 10. The convergence is rather slow; nevertheless this can be expected for system involving shallow anharmonic potentials of hydrogen bond. More disturbing, however, may seem the apparent lack of convergence of the geometry parameters. For example, the bond angle 2–3–4 changes from the initial value of ≈66.5 to ≈64.1°, but the difference for the two fragments (≈0.1°) does not seem to vanish even at later stages of the minimization. This behavior can be explained by the constraints imposed on the normal modes since these block the zero- and low-frequency motion needed for complete relaxation. Indeed, when the nor-

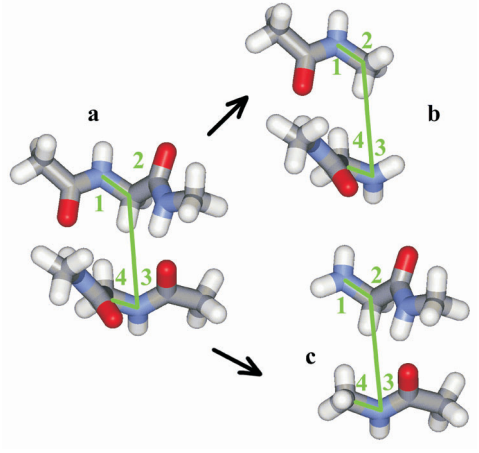

FIG. 10
The model tetraamide (a) and its decomposition into two fragments (b, c). During optimization of the fragments, the torsion angles 1–2–3–4 in the fragments were required to optimize to the same value; similarly for the distance 2–3 and bond angles 1–2–3 and 2–3–4

mal mode constraints are removed, as on the right hand side of Fig. 11, the geometry parameters converge to same values in both fragments. In the latter case, however, the convergence is even slower, as more extensive relaxation is allowed.

Minimization with Constant Potential at Nuclei

Although this advanced optimization task may find application for rather bigger molecules in solutions[37], it is illustrated for the CO and H_2O molecules. For larger systems, where the geometry relaxation caused by the field is very limited, the minimization would be much less spectacular, as it is realized mostly by rotations and translations. The external electrostatic field was modeled by two charges (0.5 e at (–2,2.5) Å and –0.5 e at (2,–2.5) Å in the *xy*-plane). The starting geometries were [C(–0.793,0.166),O(–0.116,–0.435)] for CO and [H(0.793,0.166),O(–0.116,–0.435),H(–0.676,0.269)] for the wa-

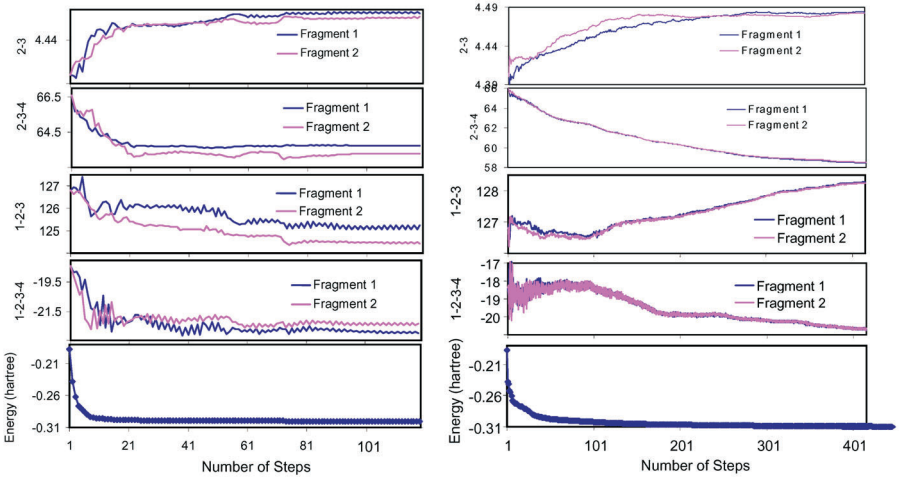

FIG. 11

Convergence of the total energy and the geometry parameters for the two molecules optimized simultaneously. The two molecules ("fragments") and the coupled geometry parameters are defined in Fig. 10. On the left-hand side of the figure, normal modes within the interval of wavenumbers (–300,300 cm^{-1}) were kept fixed while for the optimization shown on the right-hand side no normal mode restriction was applied. For both optimization runs, the penalty function was applied to the coupled distances (2–3), bond (1–2–3 and 2–3–4) and torsional (1–2–3–4) angles

ter molecule. These original parameters were relatively far from the equilibrium positions of nuclei and the molecules had to relax significantly. The BPW91/6-31G** DFT level was chosen for the optimization. As indicated above, due to the constant field condition, the rotational motions (in this case the rotation around the *y*-axis) significantly contributed to the system relaxation and could not be neglected. This can be seen in Fig. 12, where the starting and optimized geometries are overlapped. In order to optimize the higher-frequency molecular vibrations only, normal modes with frequencies below 300 cm^{-1} were frozen. If these predominantly translational modes were also allowed to relax, the CO molecule additionally shifted significantly (by ≈1.5 Å) to the region with a lower gradient of the electrostatic potential. In the final stages of the optimization where gradient becomes small, numerical instability was observed during the Hessian updating process; this could be circumvented by switching off the updating of the second derivatives in QGRAD.

CONCLUSIONS

Regarding the convergence speed the normal modes are in principle equivalent to Cartesian coordinates. For simple optimization tasks, not involving non-linear transformations, they exhibit exactly same optimization paths. Even when non-linear factors, like the RFO transformation, are involved,

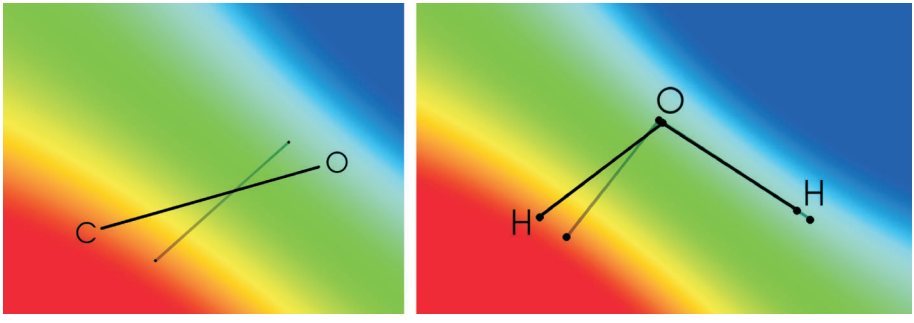

FIG. 12
Optimization of the CO and H_2O molecules under constant potential at the nuclei. By the transparent and black lines the starting and the optimized geometries are indicated, respectively. The electrostatic potentials were 0.061 and –0.026 (atomic units) for CO, and –0.033, –0.026 and 0.063 a.u. for the H, O, H atoms of H_2O. The color of the isopotential regions is chosen so that approximately the span of (–0.1,0.1 a.u.) of the potential is covered. Additionally, the dispersive normal mode motions with vibrational frequencies below 300 cm^{-1} were frozen during the optimizations

the two coordinate sets behave similarly for most systems. For flexible molecules and hydrogen-bonded clusters more significant differences were observed, in favor of the normal mode method. The use of the normal modes, however, is necessary in order to model the vibrational spectra. In this study the normal mode optimization scheme was expanded, so that multiple geometry parameters and electrostatic field at nuclei could be controlled, in addition to the vibrational motions. Furthermore, constraints involving multiple molecules were found possible. It was shown that these advanced optimizations can be utilized for practical simulations of vibrational spectra of model biopolymer compounds. The presented examples indicate a good numerical behavior of the method, although all the energy minimizations become rather lengthy for systems with anharmonic and shallow intermolecular potentials.

This work was supported by the Grant Agency of the Academy of Sciences of the Czech Republic (A4055104).

REFERENCES

1. Fletcher R.: *Practical Methods of Optimization*. Wiley, New York 1981.
2. Peng C., Ayala P. Y., Schlegel H. B., Frisch M. J.: *J. Comput. Chem.* **1996**, *17*, 49.
3. Baker J., Hehre W. J.: *J. Comput. Chem.* **1991**, *12*, 606.
4. Vreven T., Morokuma K., Farkas Ö., Schlegel H. B., Frisch M. J.: *J. Comput. Chem.* **2002**, *24*, 760.
5. Reveles J. U., Köster A. M.: *J. Comput. Chem.* **2004**, *25*, 1109.
6. Sellers H. L., Klimkowski V. J., Schäfer L.: *Chem. Phys. Lett.* **1978**, *58*, 541.
7. Pulay P., Fogarasi G., Pang F., Boggs J. E.: *J. Am. Chem. Soc.* **1979**, *101*, 2550.
8. Fogarasi G., Zhou X., Taylor P. W., Pulay P.: *J. Am. Chem. Soc.* **1992**, *114*, 8191.
9. Ahlrichs R., von Arnim M.: *J. Chem. Phys.* **1999**, *111*, **9183**.
10. Lindh R., Bernhardsson A., Schutz M.: *Chem. Phys. Lett.* **1999**, *393*, 567.
11. Baker J., Kessi A., Delley B.: *J. Chem. Phys.* **1996**, *105*, 192.
12. Schlegel H. B.: *Int. J. Quantum Chem., Quantum Chem. Symp.* **1992**, *26*, 243.
13. Baker J.: *J. Comput. Chem.* **1993**, *14*, 1085.
14. Bearpark M. J., Robb M. A., Schlegel H. B.: *Chem. Phys. Lett.* **1994**, *223*, 269.
15. Anglada J. M., Bofill J. M.: *J. Comput. Chem.* **1997**, *18*, 992.
16. Eckert F., Pulay P., Werner H. J.: *J. Comput. Chem.* **1997**, *18*, 1473.
17. Bouř P., Keiderling T. A.: *J. Chem. Phys.* **2002**, *117*, 4126.
18. Andrushchenko V., Wieser H., Bouř P.: *J. Phys. Chem. B* **2004**, *108*, 3899.
19. Bouř P., Keiderling T. A.: *J. Chem. Phys.* **2003**, *119*, 11253.
20. Bouř P.: *Chem. Phys. Lett.* **2002**, *365*, 82.
21. Ayala P. Y., Schlegel H. B.: *J. Chem. Phys.* **1997**, *107*, 375.
22. Banerjee A., Adams N., Simons J., Shepard R.: *J. Phys. Chem.* **1985**, *89*, 52.
23. Nichols J., Taylor H., Schmidt P., Simons J.: *J. Chem. Phys.* **1990**, *92*, 340.

24. Fletcher R.: *Practical Methods of Optimization: Constrained Optimization*, Vol. 2. Wiley, New York 1981.
25. van de Graaf B., Baas J. M.: *J. Comput. Chem.* **1984**, *5*, 314.
26. Baker J.: *J. Comput. Chem.* **1997**, *18*, 1079.
27. Baker J.: *J. Comput. Chem.* **1992**, *13*, 240.
28. Onsager L.: *J. Am. Chem. Soc.* **1936**, *58*, 1486.
29. Tomasi J., Mennucci B., Cancès E.: *J. Mol. Struct. (THEOCHEM)* **1999**, *464*, 211.
30. Eckert F., Klamt A.: *AIChE J.* **2002**, *48*, 369.
31. Foresman J. B., Keith T. A., Wiberg K. B., Snoonian J., Frisch M. J.: *J. Phys. Chem.* **1996**, *100*, 16098.
32. Pliego J. R., Riveros J. M.: *J. Phys. Chem. A* **2001**, *105*, 7241.
33. Mennucci B., Tomas J., Cammi R., Cheeseman J. R., Frisch M. J., Devlin F. J., Gabriel S., Stephens P. J.: *J. Phys. Chem. A* **2002**, *106*, 6102.
34. Corni S., Cappelli C., Cammi R., Tomasi J.: *J. Phys. Chem. A* **2001**, *105*, 8310.
35. Ham S., Kim J. H., Lee H., Cho M.: *J. Chem. Phys.* **2003**, *118*, 3491.
36. Cho M.: *J. Chem. Phys.* **2003**, *118*, 3480.
37. Bouř P.: *J. Chem. Phys.* **2004**, *121*, 7545.
38. Bouř P., Michalík D., Kapitán J.: *J. Chem. Phys.* **2005**, *122*, 144501.
39. Papoušek D., Aliev M. R.: *Molecular Vibrational/Rotational Spectra*. Academia, Prague 1982.
40. a) Broyden C. G.: *J. Inst. Math. Appl.* **1970**, *6*, 76; b) Fletcher R.: *Comput. J.* **1970**, *13*, 317; c) Goldfarb D.: *Math. Comput.* **1970**, *24*, 23; d) Shanno D. F.: *Math. Comput.* **1970**, *24*, 647.
41. Wilson E. B., Decius J. C., Cross P. C.: *Molecular Vibrations*. McGraw–Hill, New York 1955.
42. Klyne W., Prelog V.: *Experientia* **1960**, 521.
43. Bouř P., Tam C. N., Shaharuzzaman M., Chickos J. S., Keiderling T. A.: *J. Phys. Chem.* **1996**, *100*, 15041.
44. Frisch M. J., Trucks G. W., Schlegel H. B., Scuseria G. E., Robb M. A., Cheeseman J. R., Montgomery J. A., Vreven J. T., Kudin K. N., Burant J. C., Millam J. M., Iyengar S. S., Tomasi J., Barone V., Mennucci B., Cossi M., Scalmani G., Rega N., Petersson G. A., Nakatsuji H., Hada M., Ehara M., Toyota K., Fukuda R., Hasegawa J., Ishida M., Nakajima T., Honda Y., Kitao O., Nakai H., Klene M., Li X., Knox J. E., Hratchian H. P., Cross J. B., Adamo C., Jaramillo J., Gomperts R., Stratmann R. E., Yazyev O., Austin A. J., Cammi R., Pomelli C., Ochterski J. W., Ayala P. Y., Morokuma K., Voth G. A., Salvador P., Dannenberg J. J., Zakrzewski V. G., Dapprich S., Daniels A. D., Strain M. C., Farkas O., Malick D. K., Rabuck A. D., Raghavachari K., Foresman J. B., Ortiz J. V., Cui Q., Baboul A. G., Clifford S., Cioslowski J., Stefanov B. B., Liu G., Liashenko A., Piskorz P., Komaromi I., Martin R. L., Fox D. J., Keith T., Al-Laham M. A., Peng C. Y., Nanayakkara A., Challacombe M., Gill P. M. W., Johnson B., Chen W., Wong M. W., Gonzales C., Pople J. A.: *Gaussian 03*, Rev. B02. Gaussian, Inc., Pittsburgh (PA) 2003.
45. Shamovsky I. L., Ross G. M., Riopelle R. J.: *J. Phys. Chem. B* **2000**, *104*, 11296.
46. Kubelka J., Keiderling T. A.: *J. Am. Chem. Soc.* **2001**, *123*, 12048.
47. Bouř P., Keiderling T. A.: *J. Mol. Struct. (THEOCHEM)* **2004**, *675*, 95.
48. Creighton T. E.: *Proteins: Structures and Molecular Properties*. Freeman and Co., New York 1993.
49. Bouř P., Kubelka J., Keiderling T. A.: *Biopolymers* **2002**, *65*, 45.

50. Bouř P., Sopková J., Bednárová L., Maloň P., Keiderling T. A.: *J. Comput. Chem.* **1997**, *18*, 646.
51. Andrushchenko V., Wieser H., Bouř P.: *J. Phys. Chem. B* **2004**, *108*, 3899.
52. Andrushchenko V., Wieser H., Bouř P.: *J. Phys. Chem. B* **2002**, *106*, 12623.
53. Aravinda S., Shamala N., Rajkishore R., Gopi H. N., Balaram P.: *Angew. Chem., Int. Ed.* **2000**, *41*, 3863.
54. Cochran A. G., Skelton N. J., Starovasnik M. A.: *Proc. Natl. Acad. Sci. U.S.A.* **2001**, *98*, 5578.